Dalton Transactions

ROYAL SOCIETY OF CHEMISTRY

PAPER

View Article Online
View Journal | View Issue

Cite this: *Dalton Trans.*, 2026, **55**, 4664

Asp and His-rich model peptides as a basis for elucidating Mn(II) and Fe(II) peptide coordination chemistry

Karolina Pawlik, Malgorzata Ostrowska * and Elzbieta Gumienna-Kontecka

Although Mn(II) and Fe(II) ions are essential for all living organisms, particularly pathogenic bacteria, their coordination preferences with peptide ligands remain insufficiently understood. Building on our previous findings and inspired by naturally occurring Mn(II)- and Fe(II)-binding motifs, we designed six model peptides (L1: Ac-HDHDHDHHH-NH_2, L2: Ac-HDHDHHHHH-NH_2, L3: Ac-HDDHDDHDH-NH_2, L4: Ac-HHDDDDHHHH-NH_2, L5: Ac-HHDDDHHHH-NH_2, and L6: Ac-DDDDDD-NH_2) to explore the fundamental aspects of their metal coordination. Spectrometric, spectroscopic (electron paramagnetic resonance), and pH-potentiometric techniques were employed to determine the thermodynamic and structural properties of the resulting complexes. All studied peptides were found to form chelate complexes with Mn(II) and Fe(II) ions, although the stability of the complexes varies. Even though the protonation states of various species differ all investigated complexes remain stable in pH = 7.4. The thermodynamic stability of these complexes is strongly influenced by the peptide architecture, the number and type of potential binding residues, and the overall charge of the system. These findings provide new insights into the coordination behavior of Mn(II) and Fe(II) with histidine- and aspartic acid-rich sequences, contributing to a deeper understanding of metal ion binding in biological systems.

Received 23rd January 2026,
Accepted 21st February 2026

DOI: 10.1039/d6dt00180g

rsc.li/dalton

Introduction

Metal ions and their interactions with biologically relevant molecules are a crucial part of vast biological systems. In the context of metal–protein interactions, for over one-third of all discovered proteins, their interactions with metal ions are essential for proper function. Metal ions serve not only as cofactors, regulators and catalysts, but also possess structural functions, and govern the proper folding and conformational changes of a protein.[1] Understanding metal–protein interactions is one of the main goals of bioinorganic chemists. The best way to obtain precise information about the coordination sphere of a metal ion in a protein is through X-ray crystallography.[2] While obtaining high-quality crystals is not trivial, crystallographic data provide structural information limited to the solid state. The solution studies can aid in characterizing the protein's coordination chemistry and identifying its metal-binding sites under conditions that more closely reflect its native environment. However, due to the size of proteins and the large number of deprotonating residues they contain, studying the metal-ion binding preferences in solution can be challenging. In such cases, carefully designed model peptides mimicking binding sites of various proteins can be used as simplified protein models to understand better the factors influencing the complexation process and the coordination chemistry of the studied metal ions.[3–6]

We decided to use this approach to better understand the influence of the presence, number, and position of certain amino acids on the binding of Mn(II) and Fe(II) ions. While the coordination chemistry of Cu(II), Zn(II), or Ni(II) ions with proteins and peptides has been extensively studied for several decades, and the knowledge about the factors influencing the stability and structures of formed complexes is well-described and systematized,[7–12] there is an urgent need to deepen the knowledge about bioinorganic chemistry of Mn(II) and Fe(II) ions. These two metal ions have attracted considerable attention from researchers due to their role in almost all forms of life, especially in pathogens and in the host immune system.[13] Unfortunately, in contrast to other biologically important metal ions, there is a negligible number of papers concerning coordination, structure, and stability of Mn(II) and Fe(II)–peptide complexes.[12,14–20] There is a significant gap in understanding factors influencing the thermodynamic stability of these complexes, and systematic studies are urgently needed. Working with these metal ions can be quite challenging, for example due to the high susceptibility of Fe(II) ions to oxidation, or the limitations in use of spectroscopic methods in identifying Mn(II), or Fe(II) binding residues. However, under-

Faculty of Chemistry, University of Wrocław, 50-383 Wrocław, Poland.
E-mail: malgorzata.ostrowska3@uwr.edu.pl

standing the thermodynamic parameters of small, artificial model peptide complexes with metal ions is an important step to further analyze metal binding-structure–function relationships of naturally occurring proteins.

Sequences of model peptides designed to shed light on the bioinorganic chemistry of Mn(II) and Fe(II)–peptide complexes, described in this paper, are based on two amino acids – histidine (His) and aspartic acid (Asp). His is one of the most popular amino acids present in the binding site of a multitude of proteins.[21] The His imidazole nitrogen deprotonates just below physiological pH ($pK_a \sim 6.5$),[22–25] and allows for chelation of various metal ions, including both hard and borderline transition metal ions (in accordance with Pearson classification).[21,26] It's versatility as a metal ion binding site is evidenced in its popularity in a variety of proteins, including metallophores,[27,28] glycoproteins,[29] or various snake venoms.[30,31] The general role of His-rich sequences in nature can be described as binding metal ions, and poly-His motifs play a key part in metal ion transport and homeostasis. The number of residues and their position and are crucial factors influencing the selectivity and specificity of a protein toward metal ions.[26,32] Asp, although not as commonly present in metal-binding sites of proteins as His or cysteine, also plays an important part in biological systems. Asp-rich sequences are found in antimicrobial peptides,[33,34] prokaryotic zinc fingers,[35] and proteins involved in bone and teeth formation.[36,37] Thanks to the presence of a carboxylic group, fully deprotonated ($pK_a \sim 4$)[24] and negatively charged at pH 7.4, Asp residues can act as a ligand to chelate hard acids (Pearson classification) and electrostatically stabilize binding to positively charged metal ions. Moreover, Asp-rich regions of proteins frequently lack organized secondary or tertiary structure. The reason behind it is the electrostatic repulsion between negatively charged neighboring carboxylate groups. The presence of this amino acid in unstructured regions of proteins allows for geometric flexibility in the interactions with metal ions and impacts protein's structural dynamics, interaction capabilities, and involvement in cellular processes.[38,39]

In our previous work, we examined how the occurrence, position, and number of potential binding sites influence Mn(II) and Fe(II) complex stability, using six model peptides enriched in His, Asp, and glutamic acid (Glu) residues.[20] Our analysis showed that elongation of poly-His chains enhances metal binding, while separation of His residues by non-binding amino acid reduces stability, with distinct trends observed for all investigated metal ions. Moreover, in the case of researched model peptides, it was concluded that the presence of oxygen donor atoms in poly-His peptide sequences has a different impact on the stability of complexes depending on the metal ion. These results reveal how subtle sequence variations influence metal–peptide interactions, highlight the role of polymorphic binding, and the need for broader systematic studies to clarify general principles of Mn(II) and Fe(II) coordination in proteins. To achieve this goal, we have designed further analogues of model peptides to elucidate the influence of the number and position of Asp residues in peptide sequences (Table 1). Once again, because Zn(II) ions often coordinate to the same binding sites as Mn(II) and Fe(II), we have decided to expand our investigation to Zn(II), and to directly compare the data obtained for all studied systems. The coordination abilities, thermodynamic and structural characteristics were studied by means of mass spectrometry, potentiometric titrations, and electron paramagnetic resonance (EPR) spectroscopy.

Table 1 The sequences and the maximum protonation states of the studied model peptides

Name	Maximum protonation state	Model peptide sequence
L1	$[H_9L]^{6+}$	Ac-HDHDHDHHH-NH_2
L2	$[H_9L]^{7+}$	Ac-HDHDHHHHH-NH_2
L3	$[H_9L]^{4+}$	Ac-HDDHDDHDH-NH_2
L4	$[H_{10}L]^{6+}$	Ac-HHDDDDHHHH-NH_2
L5	$[H_9L]^{6+}$	Ac-HHDDDHHHH-NH_2
L6	$[H_6L]$	Ac-DDDDDD-NH_2

Experimental section

Materials

All ligands used in this work were purchased from KareBay and RyoBiotech and were of 98% purity. The identity of the peptides was confirmed by mass spectrometry, and their purity was examined by potentiometric titrations using the Gran method.[40] Carbonate-free 0.1 M sodium hydroxide solution was purchased from Honeywell Fluka and standardized by potentiometric titrations with potassium hydrogen phthalate (Sigma-Aldrich). Solutions containing Zn(II) and Mn(II) ions were made from corresponding metal perchlorate salts (Sigma-Aldrich) and standardized using two independent methods: inductively coupled plasma optical emission spectrometry (ICP-OES) and complexometric titrations with standardized ethylenediaminetetraacetic acid disodium salt (Na_2H_2EDTA) and murexide. Because of the high oxidation susceptibility of Fe(II) ions, solutions containing those ions were prepared and standardized in an inert atmosphere immediately before the experiments. All experiments involving Fe(II) were performed in an argon atmosphere inside a glovebox, using deoxygenated solvents. The solutions were prepared using ammonium iron (II) sulfate (Sigma-Aldrich) and standardized using 1,10-phenanthroline (Sigma-Aldrich) colorimetric assay. In mass spectrometry experiments, no peaks assigned to Fe(III) complexes were observed. During potentiometric titrations, the sample remained colorless and transparent throughout the investigated pH range. All used solutions were prepared using double-distilled water. The ionic strength of all samples was adjusted to I = 0.1 M by addition of sodium perchlorate (Sigma-Aldrich). Ligand samples also contained 4 mM of perchloric acid (J.T. Baker).

Electrospray ionization mass spectrometry (ESI-MS)

ESI-MS experiments were performed using Bruker Q-TOF compact mass spectrometer. Spectra were measured in posi-

tive-ion mode and contained a 0.1 mM concentration of ligand. Each sample was prepared in a 50 : 50 (v/v) methanol/water mixture, with 1 : 1, and 1 : 2 metal/ligand molar ratios. Each sample was measured at pH 6. The pH was adjusted by the addition of 0.1 M NH_3 solution, or 0.1 M HCl. The TuneMix mixture (Bruker Daltonics) was used to calibrate the instrument. The instrumental parameters were: scan range m/z = 250–2000; dry gas, nitrogen; T = 170 °C; capillary voltage, 4500 V; ion energy, 5 eV. The samples were infused at a flow rate of 3 μl min^{-1}. The data were processed with the use of the Compass Data Analysis 4.0 software (Bruker Daltonics). All the used solvents were of liquid chromatography-mass spectrometry grade.

Potentiometric titrations

Potentiometric titrations were performed using a Metrohm OMNIS titrator connected to the OMNIS dosing module. The pH of a solution was measured by a pH electrode, Micro pH-electrode (Metrohm). The glass cell used for measurements was equipped with a microstirrer, a microburette delivery tube, and an inlet–outlet tube for argon. All titrations were performed under an argon atmosphere, using a standardized (0.1 M) carbonate-free solution of sodium hydroxide as a titrant (Honeywell Fluka). The electrode was calibrated daily for hydrogen ion concentration by performing at least three titrations of 3 ml of 4 mM perchloric acid solution with sodium hydroxide (I = 0.1 M $NaClO_4$). The electrode characteristic, such as standard potential, and slope were computed by means of the GLEE program.[41] L1–L5 solutions contained 0.5 mM, and L6 solutions contained 1 mM of ligand; all solutions contained 4 mM concentrations of perchloric acid, and 0.1 M concentrations of sodium perchlorate (ionic strength). The titrated sample volume was 3 ml. The measurements of metal–ligand complexes were performed at a 1 : 1.1 (metal/ligand) molar ratio for L1–L5, and 1 : 1.1 and 1 : 2 ratio for L6. The precise concentrations of ligand solutions were determined using the Gran method.[23] All stability constants of proton and metal–ligand complexes were calculated using titration curves obtained at 298 K and in the 2–11 pH range using HYPERQUAD 2008 [42] software. The competition and speciation diagrams were created using HYSS[43] and OriginLab 2016 software. The Mn(II), Fe(II), and Zn(II) hydrolysis constants were taken into consideration during stability constant calculations of metal–ligand complexes. The constants at zero ionic strength were obtained from The hydrolysis of metal cations by Brown and Ekberg[44] and calculated to 0.1 M ionic strength with the formula proposed by Baes and Mesmer (Table S1).[45]

Electron paramagnetic resonance (EPR) spectroscopy

EPR spectra were recorded using a Bruker ELEXSYS E500 CW-EPR spectrometer equipped with an NMR teslameter (ER 036TM) and a frequency counter (E 41 FC) at X-band frequency at room temperature (298 K). The ligand concentration was 0.5 mM, and the metal/ligand molar ratio was 1 : 1.1. EPR parameters were obtained by using the Doublet New (EPR OF; S = 1/2) program by A. Ozarowski (National High Field Magnetic Laboratory, University of Florida, Gainesville, FL).

Results and discussion

Ligand deprotonation constants

The dissociation constants of both free and complexed ligands were calculated from data obtained using potentiometric titrations. All investigated ligands were protected by acetylation (N-terminus), and amidation (C-terminus).

For the studied ligands, the pK_a values of the Asp lie in the range of 2.03–5.37, and the deprotonation of the imidazole groups of His occurs in the range of 5.20–7.94. These values, as well as the deprotonation patterns, remain in agreement with the literature data.[20,33,46–48] The exact pK_a values of all ligands are listed in Table 2, and speciation diagrams are presented in Fig. S1 (SI).

All ligands that contain His residues (L1–L5) undergo the formation of highly charged species at acidic pH (Table 1). The high positive charge of those species deems them less stable, favoring proton dissociation to increase the stability of the system. That is why the amino acids present in studied ligands tend to have more acidic dissociation constants, than free amino acids (pK_a 3.86 for Asp, and 6.07 for His).[24,49] The subsequent deprotonations of those ligands decrease the charge, and increase the stability of the species, and thus increase the pK_as of the following deprotonated amino acids.[50]

Metal complex stoichiometry

The stoichiometry of the studied metal–ligand complexes was obtained by means of mass spectrometry. The measurements were carried out in 1 : 1 and 1 : 2 (metal/ligand) molar ratios, at pH ~ 6. The spectra revealed the presence of three main types of ions – the ligand, metal–ligand complexes, and adducts with common ions such as Cl^-, ClO_4^-, Na^+, K^+, with varied protonation states (Fig. S2). In addition to peaks associated with mononuclear complexes, we have also observed low intensity peaks that can be assigned to binuclear complexes (M_2L) on the spectra of metal complexes of almost all ligands (Fig. S2 and S3). The formation of binuclear complexes is possible, as every studied ligand possesses multiple potential metal-binding sites. We are aware that the intensity of the obtained signals does not correlate with the concentration of the species, but with the molecules' ability to ionize. We decided to compare the intensity of the obtained ML and M_2L signals, as the they are very similar, and possess identical charges; thus their ionization abilities should be somewhat comparable. The intensity ratio in which both species are present will reveal their approximate abundance. As the intensity ratio for all observed peaks assigned to binuclear species is in the range 4 : 1–10 : 1 ($ML : M_2L$), the obtained results suggest only marginal formation of binuclear complexes (Fig. S3). Additionally, in L6 measurements, we have encountered peaks, assigned to 1 : 2 (metal/ligand) complexes (ML_2) and adducts, in which two ligands associate with each other

Table 2 Protonation constants (log β) and pK_a values of the L1–L6 ligands[a]

Assignments[b,c]	L1	L2	L3	L4	L5	L6
log $\beta(H_{10}L)$	—	—	—	54.42(5)	—	—
log $\beta(H_9L)$	48.24(3)	51.26(3)	45.84(2)	52.09(2)	50.12(2)	—
log $\beta(H_8L)$	46.21(3)	48.54(3)	43.48(2)	48.73(2)	47.84(2)	—
log $\beta(H_7L)$	43.18(3)	44.89(3)	40.65(2)	45.05(2)	44.46(2)	—
log $\beta(H_6L)$	39.39(2)	39.68(3)	37.10(2)	40.73(2)	40.45(2)	26.39(2)
log $\beta(H_5L)$	34.18(3)	34.03(5)	33.12(2)	35.07(2)	34.82(2)	22.74(6)
log $\beta(H_4L)$	28.18(3)	27.96(5)	28.42(2)	28.91(2)	28.79(2)	19.12(3)
log $\beta(H_3L)$	21.90(4)	21.62(5)	22.14(2)	22.31(2)	22.18(2)	14.80(6)
log $\beta(H_2L)$	15.04(3)	14.84(4)	15.33(2)	15.36(2)	15.34(2)	10.36(2)
log β(HL)	7.91(3)	7.74(4)	7.94(2)	7.93(5)	7.92(7)	5.37(4)
pK_a	—	—	—	2.33 (D)	—	—
pK_a	2.03 (D)	2.72 (D)	2.36 (D)	3.36 (D)	2.28 (D)	—
pK_a	3.03 (D)	3.66 (D)	2.86 (D)	3.68 (D)	3.38 (D)	—
pK_a	3.79 (D)	5.20 (H)	3.55 (D)	4.32 (D)	4.01 (D)	—
pK_a	5.21 (H)	5.65 (H)	3.98 (D)	5.66 (H)	5.63 (H)	3.64 (D)
pK_a	6.00 (H)	6.07 (H)	4.70 (D)	6.16 (H)	6.03 (H)	3.61 (D)
pK_a	6.28 (H)	6.34 (H)	6.28 (H)	6.60 (H)	6.61 (H)	4.32 (D)
pK_a	6.86 (H)	6.80 (H)	6.81 (H)	6.95 (H)	6.84 (H)	4.43 (D)
pK_a	7.13 (H)	7.10 (H)	7.39 (H)	7.43 (H)	7.42 (H)	4.99 (D)
pK_a	7.91 (H)	7.74 (H)	7.94 (H)	7.93 (H)	7.92 (H)	5.37 (D)

[a] T = 298 K, I = 0.1 M $NaClO_4$, standard deviations on the last digit given in parentheses. [b] Overall stability constants (β) expressed by the equation: $\beta(H_nL) = [H_nL]/[L][H^+]^n$. [c] Acid dissociation constants (pK_a) expressed as: pK_a = log $\beta(H_nL)$ − log $\beta(H_{n-1}L)$.

(L_2) (Fig. S4). Those peaks were unique for L6 ligand, and the ratio of ML : ML_2 was around 2 : 1, depending on the spectrum. Since L6 is the only all-Asp ligand we have examined, we suspect the L_2 adduct may be a result of this specific ligand composition.

Metal complex thermodynamic stability and structure

For all ligands, the potentiometric titration calculations suggest the formation of mononuclear species, with varying protonation states as shown in Table 1. The species distributions of the studied ligands are presented in Fig. S1. The possibility of polynuclear species being present in the solution was considered (*vide supra*), but those forms were rejected from the proposed potentiometric models by the program used for calculations. Moreover, potentiometric titrations in excess of metal ions are not possible due to the increase in metal ions' hydrolysis, resulting in the precipitation of insoluble hydroxides. For L6 the traces of bis-complexes were discovered in ESI-MS spectra (Fig. S4). For this reason, potentiometric titrations with twofold excess of the L6 ligand were conducted for all studied metal ions. Based on the traces of bis-complexes in the ESI-MS spectra, we have attempted to calculate potentiometric models for both the mixed 1 : 1 and 1 : 2 (metal/ligand), and 1 : 2 (metal/ligand) complexes for L6. The obtained fit of experimental and simulated curves was not satisfactory; thus we have assumed no bis-complexes present.

Mn(II) complexes

Due to the lack of spectroscopic information, we can only speculate about the exact number of Asp and His involved in Mn(II) binding. However, by analyzing the differences between the dissociation constants of complexed and free ligands, we could obtain information about the involvement of specific residues in the metal ion binding. Usually, by comparing the pK_a of a residue present in the complex with the corresponding pK_a of the free ligand we can determine its engagement in metal binding. The binding of the metal ion is signified by the decrease in pK_a of the analyzed residue. We present a detailed analysis only of L1's deprotonation pattern, as the aim of this paper is to identify broader trends in Mn(II) and Fe(II) peptide complex formation, not the detailed deprotonation pattern analysis of each ligand. The same methodology was employed to analyze the complexes formed with remaining ligands.

For L1 (Ac-HDHDHDHHH-NH_2) the complexation process begins at pH ∼ 3 with the deprotonation of all 3 Asp residues present in the ligand, and a single His residue (Table 3 and Fig. 1). Due to the non-stepwise deprotonation pattern for this ligand, the determination of exact dissociation constants is not possible for most residues. We can discuss only the second deprotonated His, for which the pK_a is decreased by 0.35 in comparison to the free ligand's. This decrease suggests binding of said residue. Subsequent proton dissociation events involve the joined deprotonation of pairs of His, up to achieving [MnL] form. The last deprotonation is the loss of a proton, most probably from a water molecule, resulting in the formation of $[MnLH_{-1}]$ species.

Taking our latest findings,[20] together with the analysis performed in this paper and the literature data on Mn(II) complexes with poly-His peptides, we can propose Mn(II) complexation by two, or three separated imidazole groups.[51–53] The presence of multiple complex species remaining in equilibrium, characterized by distinct arrangements of imidazole nitrogen atoms coordinating the Mn(II) ion, is known in the literature as a so called "polymorphic binding site".[11,30,51] Based on the analysis of the available deprotonation constants and

Table 3 Stability constants (log β), and pK_a values of all Mn(II)/peptide systems[a]

Assignments [b,c]	L1	L2	L3	L4	L5	L6
log β [MnH_6L]	—	43.38(6)	—	44.44(7)	43.86(4)	—
log β [MnH_5L]	37.87(9)	—	—	39.24(9)	39.07(4)	—
log β [MnH_4L]	32.26(7)	32.01(5)	31.90(4)	33.49(7)	—	21.46(4)
log β [MnH_3L]	—	—	26.20(5)	—	26.90(3)	—
log β [MnH_2L]	19.65(6)	19.07(5)	19.53(4)	20.45(7)	—	13.50(2)
log β [MnHL]	—	—	12.41(5)	—	12.86(4)	—
log β [MnL]	5.07(6)	4.43(5)	4.98(3)	5.46(7)	4.82(4)	3.92(2)
log β [$MnLH_{-1}$]	−4.30(5)	−5.07(4)	−4.37(4)	−4.00(9)	−4.88(5)	−2.01(3)
log β [$MnLH_{-2}$]	—	—	—	—	—	−11.75(7)
log β [$MnLH_{-3}$]	—	—	−26.10(3)	−24.35(8)	−25.79(4)	−21.67(3)
pK_a [MnH_6L]		—	—	—	—	—
pK_a [MnH_5L]	—	—	—	5.20	4.79	—
pK_a [MnH_4L]	5.61	—	—	5.75	—	—
pK_a [MnH_3L]	—	—	5.70	—	—	—
pK_a [MnH_2L]	—	—	6.67	—	—	—
pK_a [MnHL]	—	—	7.12	—	—	—
pK_a [MnL]	—	—	7.43	—	8.04	—
pK_a [$MnLH_{-1}$]	9.37	9.50	9.35	9.46	9.70	5.93
pK_a [$MnLH_{-2}$]	—	—	—	—	—	9.73
pK_a [$MnLH_{-3}$]	—	—	—	—	—	9.92

[a] T = 298 K, I = 0.1 M $NaClO_4$, standard deviations on the last digit given in parentheses. [b] Overall stability constants (β) expressed by the equation: $\beta([MnH_nL]^{(n+2)+}) = [[MnH_nL]^{(n+2)+}]/[Mn(II)][[L]^{n+}][H^+]^n$. [c] Acid dissociation constants (pK_a) expressed as: pK_a = log $\beta([MnH_nL]^{(n+2)+})$ − log $\beta([MnH_{n-1}L]^{(n+1)+})$.

the deprotonation patterns (Table 3), we suspect the binding mode for L1 to be {3COO$^-$, 2N_{im}, H_2O}, or {2COO$^-$, 3N_{im}, H_2O}. The same analysis led us to propose {2COO$^-$, 3N_{im}, H_2O} binding mode for L2; and {3N_{im}, 3H_2O} for L3–L5 ligands.

For the last studied ligand (L6), which consists of six Asp residues, the exact number of binding residues is also unknown, due to the non-stepwise ligand deprotonation. The subsequent species, such as [$MnLH_{-1}$], [$MnLH_{-2}$] and [$MnLH_{-3}$] are, most probably, the effects of water molecules deprotonation from the metal ion coordination sphere. Considering the number of deprotonated water molecules, a {3COO$^-$, 3H_2O} coordination mode can be proposed beginning from the $[MnH_2L]^{2-}$ species.

Room temperature electron paramagnetic resonance (RT EPR, T = 298 K) measurements were employed to confirm the formation of Mn(II)-peptide complexes. The experiments were conducted in a broad pH range of ~2–11 (Fig. S5). Mn(II) is a high spin paramagnetic metal ion, possessing a $3d^5$ valence electron configuration, with the spin state S = 5/2, and the nuclear spin state I = 5/2. For high-spin Mn(II) complexes we observe a very small anisotropy of the Zeeman interactions, which leads to a small g value, similar to that of a free electron (g = 2.0023). This behavior is typical for S-state ions with spherical electron-density geometry.

At room temperature (RT), the $[Mn(H_2O)_6]^{2+}$ complex displays a characteristic six-line X-band EPR spectrum centered at g = 2.002, due to hyperfine splitting of the allowed EPR transition. When the coordinated water molecules are replaced by peptide side chains, this signal weakens (Fig. S5). Mn(II) ions bound to peptides become EPR silent at RT because the signal broadens beyond detection. This broadening results from zero-field splitting, which is induced by changes in the ligand field around the Mn(II) center. Therefore, the detectable RT EPR signal originates exclusively from unbound Mn(II) ions. The progressive loss of signal intensity with increasing pH indicates the binding of Mn(II) ions to the peptides.

Fe(II) complexes

Using the same line of reasoning as described for Mn(II) complexes, by comparing the deprotonation constants of complexed and free ligands when it was possible, we aimed to determine the possible coordination model of each of studied peptides with Fe(II) ions.

For most described complexes, the non-stepwise deprotonation patterns and the lack of deprotonation constants hinder the analysis, making the speculation on their binding mode quite challenging. Based on our analysis (Table 4 and Fig. 2) the coordination by 2 or 3N_{im} is the most probable for L1–L5 ligands, together with the 4 (L1), or 3 (L2–L5) additional deprotonation steps, not observed in a free ligand. This additional deprotonation steps are commonly associated with deprotonation of water molecules or amide nitrogens in coordination sphere of metal ions. In the case of Fe(II) ions, we have no direct confirmation or denial of the possibility of coordination of amide nitrogen to the metal ion, and further investigations are needed. Taking the number of deprotonated water molecules/amide nitrogens into account, we can suspect the {2N_{im}, 4H_2O/4N_{amide}} coordination for L1, and {3N_{im}, 3H_2O/3N_{amide}} coordination for L2–L5 ligands. The proposed coordination mode for L6 is heavily based on the number of deprotonating water/amide molecules, and suggests {2COO$^-$, 4H_2O/4N_{amide}} binding. Moreover, analysis of the deprotonation patterns of all studied complexes suggests the occurrence of the previously mentioned "polymorphic binding site" phenomenon.

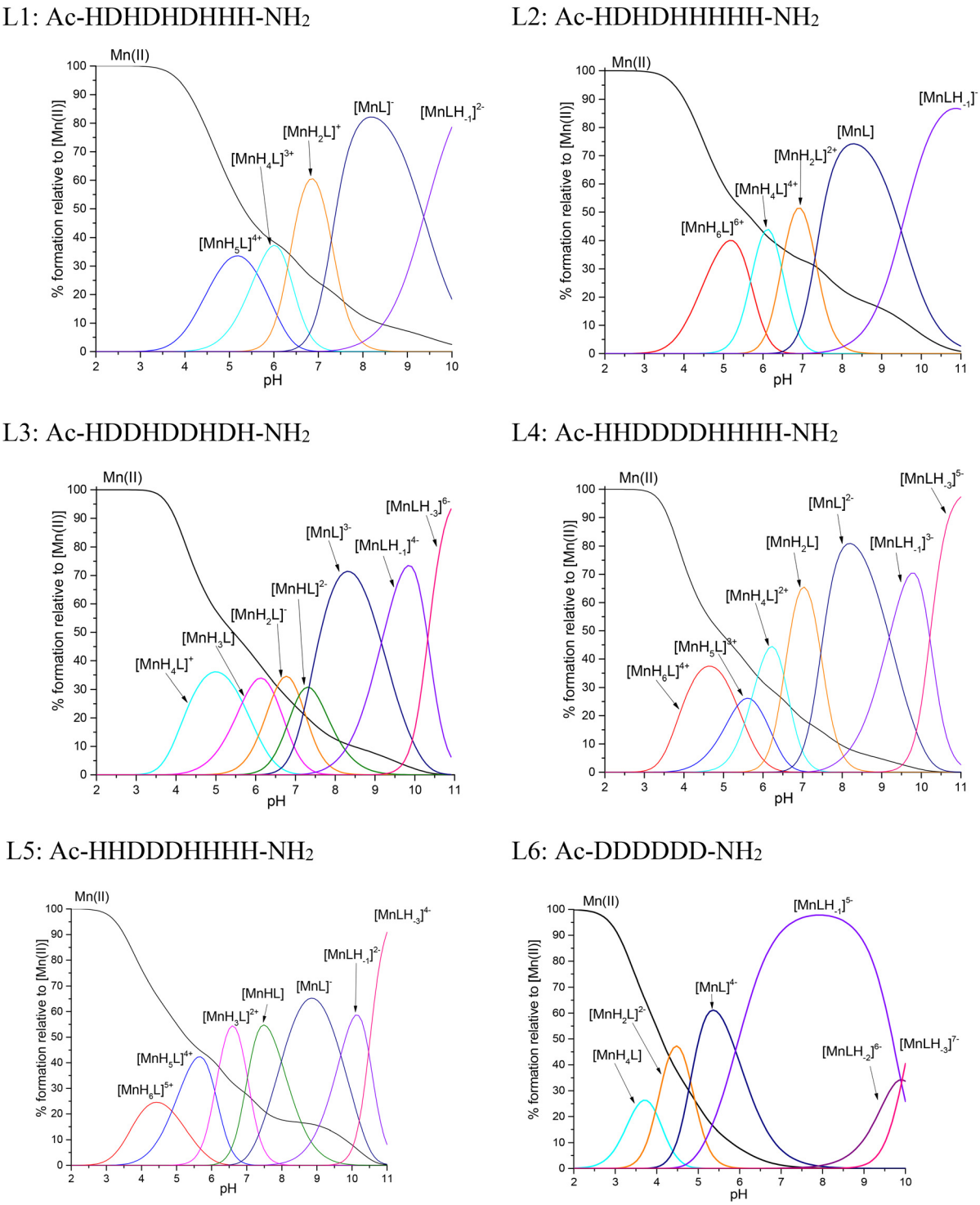

Fig. 1 Species distribution diagrams of complexes formed between Mn(II) and L1–L6 systems. Species distribution calculated for potentiometric titration experimental conditions. $[Mn(II)]_{tot}$ = 0.45 mM; M : L = 1 : 1.1 for L1–L5; $[Mn(II)_{tot}]$ = 0.5 mM; M : L = 1 : 2 for L6.

Zn(II) complexes

The analysis of Zn(II) complexes have been conducted in a similar manner as previously described for Mn(II) and Fe(II) complexes, and can be found in the SI for this work, together with the stability constants and pK_a values of all Zn(II) complexes (Table S2), and the species distribution diagrams (Fig. S6). The obtained results are in good agreement with literature data described for similar poly-His and poly-Asp peptide ligands.[11,28,54,55]

Table 4 Stability constants (log β), and pK_a values of all Fe(II)/peptide systems[a]

Assignments[b,c]	L1	L2	L3	L4	L5	L6
log β [FeH_6L]	42.98(4)	—	—	—	—	—
log β [FeH_5L]	38.46(4)	—	—	—	—	—
log β [FeH_4L]	—	32.37(4)	—	32.39(6)	32.21(4)	22.41(4)
log β [FeH_3L]	26.70(3)	—	26.56(4)	—	—	—
log β [FeH_2L]	—	19.56(4)	20.05(3)	19.86(3)	19.49(3)	14.30(2)
log β [FeHL]	13.13(3)	12.24(9)	13.27(3)	—	12.34(4)	—
log β [FeL]	5.38(4)	4.85(7)	5.58(4)	5.48(3)	5.15(2)	4.39(2)
log β [$FeLH_{-1}$]	−2.91(4)	−3.26(6)	−2.14(3)	—	−3.14(2)	—
log β [$FeLH_{-2}$]	—	−12.46(7)	−10.77(4)	−12.07(4)	—	−11.49(4)
log β [$FeLH_{-3}$]	−21.70(4)	−21.96(6)	−19.80(4)	−21.26(3)	−21.28(2)	—
log β [$FeLH_{-4}$]	−32.20(4)	—	—	—	—	−29.09(4)
pK_a [FeH_6L]	—	—	—	—	—	—
pK_a [FeH_5L]	4.52	—	—	—	—	—
pK_a [FeH_4L]	—	—	—	—	—	—
pK_a [FeH_3L]	—	—	—	—	—	—
pK_a [FeH_2L]	—	—	6.51	—	—	—
pK_a [FeHL]	—	7.32	6.78	—	7.15	—
pK_a [FeL]	7.75	7.39	7.69	—	7.19	—
pK_a [$FeLH_{-1}$]	8.29	8.11	7.72	—	8.29	—
pK_a [$FeLH_{-2}$]	—	9.20	8.63	—	—	—
pK_a [$FeLH_{-3}$]	—	9.50	9.13	9.29	—	—
pK_a [$FeLH_{-4}$]	10.5	—	—	—	—	—

[a] T = 298 K, I = 0.1 M $NaClO_4$, standard deviations on the last digit given in parentheses. [b] Overall stability constants (β) expressed by the equation: $\beta([FeH_nL]^{(n+2)+}) = [[FeH_nL]^{(n+2)+}]/[Fe(II)][[L]^{n+}][H^+]^n$. [c] Acid dissociation constants (pK_a) expressed as: pK_a = log$\beta([FeH_nL]^{(n+2)+})$ − log$\beta([FeH_{n-1}L]^{(n+1)+})$.

Comparison of the thermodynamic stabilities of metal complexes

The thermodynamic stability of a metal–ligand complex can be described using a variety of different tools. The most popular tool for assessing the thermodynamic stability of a complex, directly describing the binding affinity between a metal ion and a ligand, is called overall stability constant of a complex (log β). However, the comparison of log β between different ligands, varying in the number and position of binding groups, is not appropriate, as the differences in ligand deprotonation constants may influence the outcome. A much safer tool for assessing the different binding power of a variety of ligands is the competition plot. The plot visualizes a hypothetical situation in which an equimolar amount of each component is present.

To draw further conclusions on the binding preferences of Mn(II) and Fe(II) ions we have decided to compare the peptides described in this paper to the strongest metal chelating peptides investigated in our previous study – namely L2*: Ac-HHHHHHHHHH-NH_2 and L5*: Ac-HDHDHDHDH-NH_2 (Scheme 1).[20] The chosen comparisons were: L2*/L5*/L1/L2 – to explore the influence of the number of Asp residues, and their specific positioning on the stability of created complexes (Fig. 3); L5*/L3/L4/L5 and L2*/L5*/L4/L6 – to explore the influence of the presence of alternating, and clustered His/Asp residues on complex stability, and to further investigate coordination preferences of both metal ions for nitrogen or oxygen donor atoms (Fig. 4 and 5).

Due to the limited understanding of Mn(II) and Fe(II) ions coordination chemistry, only the competitions for these metal ions will be discussed in detail in the main text. Zn(II) was selected for this study not only for its ability to bind to the same sites, but also as a reference for the calculations regarding Mn(II) and Fe(II) ions. Competitions regarding the Zn(II) ions (Fig. S7) are generally in good agreement with literature and well established knowledge of Zn(II) preferences; therefore they will not be discussed in detail.[11,28,54,55] However, this agreement strengthens our confidence in the calculations performed for Mn(II) and Fe(II) ions. The short summary regarding Zn(II) can be found in the SI (page S8–S13).

L2*/L5*/L1/L2

For Mn(II) ions, the number of available Asp residues correlates with complex stability, particularly in the acidic (pH < 5.75) and basic (pH > 8) ranges. The L5* ligand (Ac-HDHDHDHDH-NH_2), containing four Asp residues, displays the highest stability of all Asp-containing peptides up to ~pH 5 (Fig. 3). The trend, observed until pH 5, is in agreement with the number of deprotonated Asp residues available for binding of Mn(II) ions (4Asp for L5*; 3Asp, 1His for L1; 2Asp, 1His for L2; and 3His for L2*). Above pH 5, deprotonation of subsequent histidyl residues occurs, and from this point, the interplay between the number of possible binding His residues and the overall charge of the deprotonated ligand starts to influence the stability of the formed complexes. Around pH 5.75, L2* becomes dominant. This ligand is characterized by polymorphic binding, involving multiple His pairs, or triads. As discussed in our previous paper, above pH 5.5, the L2* ligand possesses the highest number of deprotonated His residues, with five deprotonated His available for coordination. In

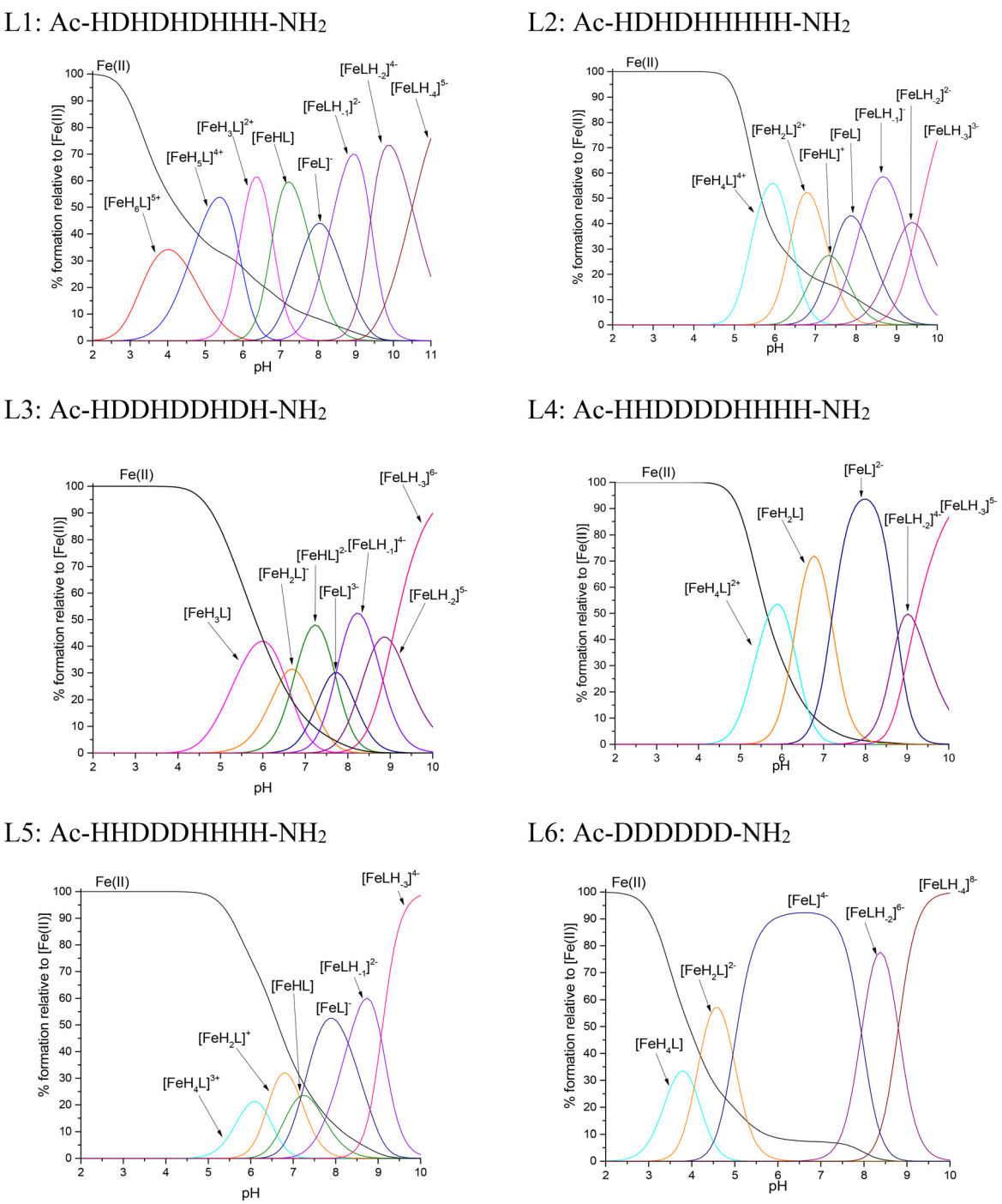

Fig. 2 Species distribution diagrams of complexes formed between Fe(II) and L1–L6 systems. Species distribution calculated for potentiometric titration experimental conditions. $[Fe(II)]_{tot}$ = 0.45 mM; M : L = 1 : 1.1 for L1–L5; $[Fe(II)_{tot}]$ = 0.5 mM; M : L = 1 : 2 for L6.

comparison, other ligands such as L1, L2, and L5* possess only 2, or 3 deprotonated His residues in the same pH range. A higher number of potential binding sites increases the stability of the resulting complex, as it allows for greater flexibility and a wider range of coordination possibilities with the metal ion. The polymorphic binding appears to result in higher stability, persisting up to ~pH 8–8.5. This trend confirms our observations regarding Mn(II)'s preferences from the previous work – the occurrence of oxygen donor atoms within poly-His peptide sequences has little influence on the ligand's affinity for Mn(II) ions around neutral pH (pH range 6–8). Instead, the existence of multiple potential binding modes, referred to as "polymorphic binding sites", was found to enhance the stability of the resulting complexes more effectively than the simple

Competition 1: **L2*/L5*/L1/L2**	L2*: Ac-HHHHHHHHHH-NH_2 L5*: Ac-HDHDHDHDH-NH_2 L1: Ac-HDHDHDHHH-NH_2 L2: Ac-HDHDHHHHH-NH_2	The influence of the number and position of His and Asp residues on complex stability.
Competition 2: **L5*/L3/L4/L5**	L5*: Ac- HDHDHDHDH-NH_2 L3: Ac-HDDHDDHDH-NH_2 L4: Ac-HHDDDDHHHH-NH_2 L5: Ac-HHDDDHHHH-NH_2	The influence of the presence of alternating and clustered His/Asp residues on complex stability.
Competition 3: **L2*/L5*/L4/L6**	L2*: Ac-HHHHHHHHHH-NH_2 L5*: Ac-HDHDHDHDH-NH_2 L4: Ac-HHDDDDHHHH-NH_2 L6: Ac-DDDDDD-NH_2	

Scheme 1 The scheme summarizes the types of peptides used in each competition, with the explanation behind the choice of competing peptides.

presence of favorable oxygen donors. Above pH 8, when all of the residues are deprotonated, and water molecules in the coordination sphere of Mn(II) ions start to deprotonate, the stability of complexes increases with the number of Asp and His pairs in the ligand, most probably due to the stabilizing effect of the overall charge of the formed complexes.

The general conclusion drawn from this competition may be that in acidic and basic pH the number of Asp increases the complex stability, but in neutral pH the Mn(II) ions present a clear preference for poly-His motif. In this range, the polymorphic His binding further stabilizes the complex by providing multiple binding sites. High lability of Mn(II) ions could promote the tendency to move along the peptide sequence and bind in various domains along the sequence and therefore form polymorphic states.

The ligand preference of Fe(II) ions shows subtle differences compared to the previously described Mn(II) system. Across the entire pH range, the competition is primarily dominated by L5* and L1, and the binding abilities of both ligands are comparable up to pH 7.2. Above this pH, the L5* clearly dominates, indicating that the alternating His–Asp sequence provides an advantageous coordination environment, likely due to the favorable electrostatic interactions. Both L2* and L2 perform poorly in this competition, most probably due to their low Asp content and high overall charge. These results suggest that although formally classified as borderline acid, according to HSAB theory, Fe(II) ions exhibit a marked preference for mixed nitrogen/oxygen donors, favoring ligands with alternating Asp–His motifs over those with His-rich clusters. It is in agreement with Fe(II) binding sites found in the literature, where one can find oxygen donor atoms in the coordination spheres of Fe(II) ions.[56] This underscores the importance of both residue type and sequence pattern in stabilizing Fe(II) complexes.[57] Additionally, we do not observe the preference for the poly-His motif here. As we do not have a direct proof, we can just speculate that Fe(II) ions do not prefer polymorphic binding states. Further studies are necessary to have deeper insights into this behavior.

The differences in Mn(II) and Fe(II) preferences for clustered and separated binding motifs, and thus polymorphic binding, may arise from their fundamental coordination chemistry. Most of the complexes of both investigated metal ions are high-spin (HS) and typically octahedral.[57,58] Due to the large effective ionic radius for HS octahedral complexes (0.83 Å)[59] and d^5 electronic configuration of Mn(II) ions, in most cases their ligand field stabilization energy is considered as 0.[57,58,60] Mn(II) ions acquire a perfectly spherical electronic shape, due to their half-filled d^5 configuration and the resulting lack of

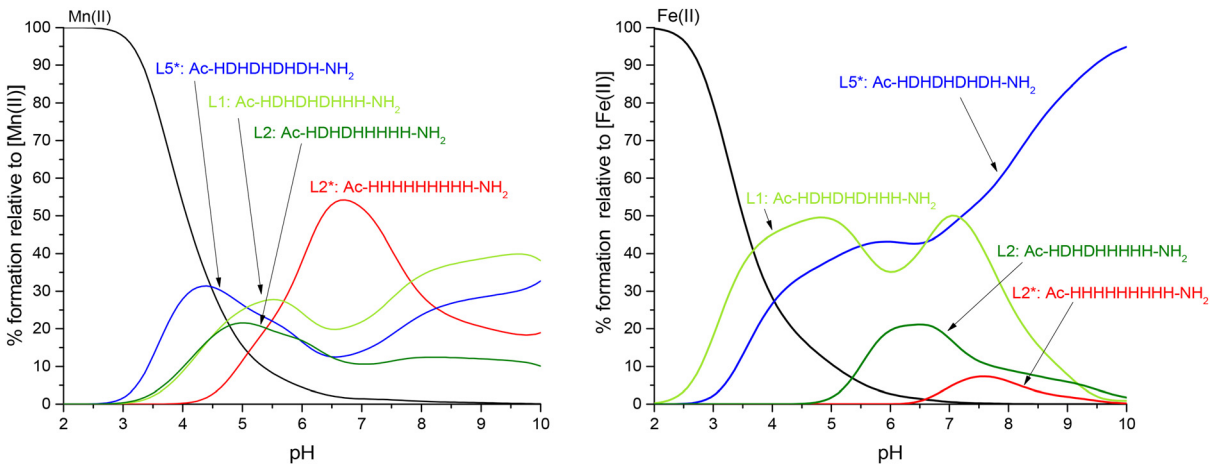

Fig. 3 Competition plots between the L2*/L5*/L1/L2 ligands and the metal ion. It describes complex formation at different pH values in a hypothetical situation in which equimolar amounts of all reagents are mixed. Calculations are based on potentiometric data from Tables 2–4 and ref. 20. The left plot presents Mn(II) systems, and the right plot presents Fe(II) systems. Conditions: T = 298 K, I = 0.1 M $NaClO_4$; the concentration of all reagents is 1×10^{-3} M.

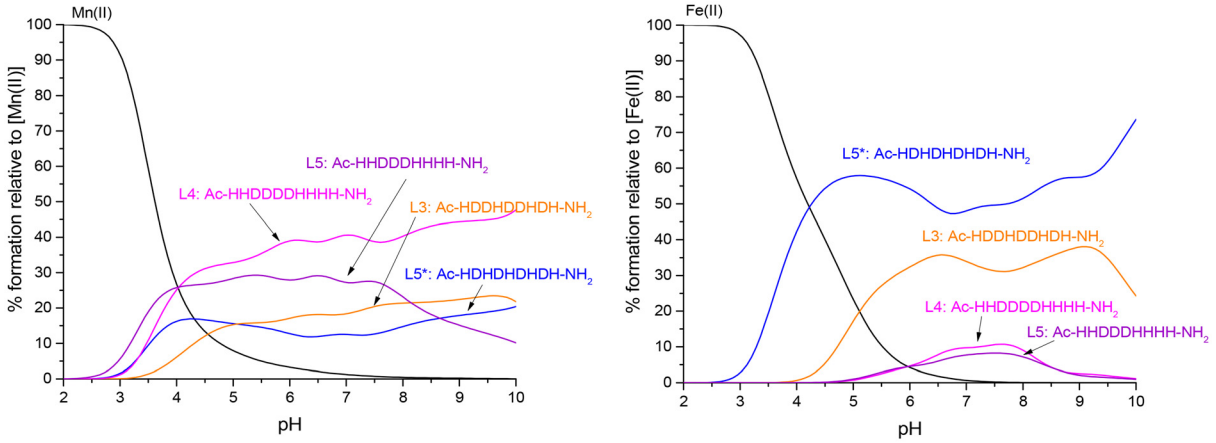

Fig. 4 Competition plots between the L5*/L3/L4/L5 ligands and the metal ion. It describes complex formation at different pH values in a hypothetical situation in which equimolar amounts of all reagents are mixed. Calculations are based on potentiometric data from Tables 2–4 and ref. 20. The left plot presents Mn(II) systems, and the right plot presents Fe(II) systems. Conditions: T = 298 K, I = 0.1 M $NaClO_4$; the concentration of all reagents is 1×10^{-3} M.

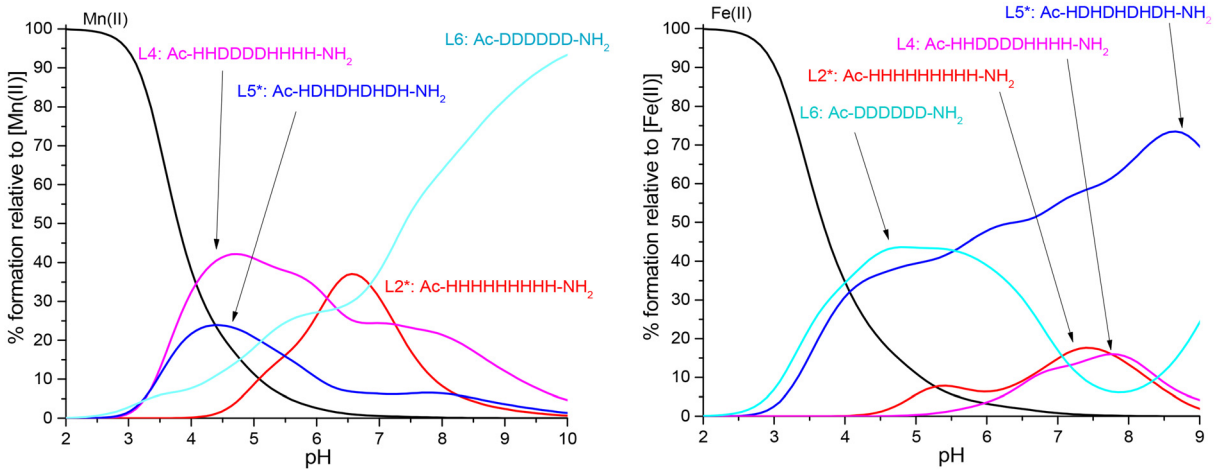

Fig. 5 Competition plots between the L2*/L5*/L4/L6 ligands and the metal ion. It describes complex formation at different pH values in a hypothetical situation in which equimolar amounts of all reagents are mixed. Calculations are based on potentiometric data from Tables 2–4 and ref. 20. The left plot presents Mn(II) systems, and the right plot presents Fe(II) systems. Conditions: T = 298 K, I = 0.1 M $NaClO_4$; the concentration of all reagents is 1×10^{-3} M.

Jahn–Teller distortion. This symmetry greatly influences Mn(II) ions flexibility concerning coordination geometry.[57,58] The difference between the ligand field stabilization energy of the reacting complex and that of the transition state influences the kinetic lability of the complexes. This difference is known as the ligand field activation energy. Both the reacting complex ligand field stabilization energy and the transition state ligand field stabilization energy are 0 for HS Mn(II) ions, making the ligand field activation energy also 0. Consequently, Mn(II) ions are the most kinetically labile of all 3d transition metal ions.[60] No ligand field activation energy for Mn(II) ions contributes to its high geometrical flexibility, allowing for coordination to be dictated by the ligand. This high geometrical flexibility, together with high lability, may explain the preference of Mn (II) ions toward ligands possessing more clustered motifs. The Mn(II) ions may bind different sets of amino acid residues within one ligand, and by that find the most suitable geometry, improving the complex stability.

For smaller, HS d^6 Fe(II) ions (0.78 Å),[59] their ligand field stabilization energy is >0. This positive ligand field stabilization energy deems the kinetic lability and geometrical flexibility of Fe(II) ions as lower than Mn(II) ions. Additionally, the octahedral, HS Fe(II) ions may be subject to a minor Jahn–Teller distortion, proving their ability to form complexes with non-ideal geometry. The preference of Fe(II) ions for ligands with neighboring Asp/His motifs may arise from both the preference for more rigid complex formation and the favorable electrostatic interactions.[57,58,60]

L5*/L3/L4/L5

This competition further emphasizes the influence of ligand architecture on complex stability. The ligands examined here represent both alternating (L5*: Ac-HDHDHDHDH-NH_2) and clustered architectures of varying sizes (L3: Ac-HDDHDDHDH-NH_2, L4: Ac-HHDDDDHHHH-NH_2, L5: Ac-HHDDDHHHH-NH_2). For Mn(II) ions, a slight preference for L4 and L5 ligands is observed. The comparison across ligands suggests that larger clusters generally confer greater complex stability. These findings support the observations that Mn(II) ions favor coordination to clustered Asp/His motifs, likely due to the potential for polymorphic binding.

Fe(II) ions exhibit distinctly different, if not opposite, coordination preferences compared to Mn(II). As shown in the competition plot (Fig. 4), Fe(II) displays a strong preference for L5*, which features an alternating Asp–His motif and forms significantly more stable complexes than the other ligands. This may be explained by looking into basic coordination chemistry of both metal ions (*vide supra*), combined with the geometric flexibility of Asp-rich peptides (as explained in the Introduction) and the electrostatically favorable interactions between His/Asp pairs. Among the ligands with clustered residues, L3 (containing the smallest clusters) performs best, while both L4 (4 Asp cluster) and L5 (3 Asp cluster) show similarly low stability. Overall, the results suggest a decrease in complex stability with increasing cluster size.

L2*/L5*/L4/L6

For Mn(II) complexes, all Asp-bearing ligands (L4, L5*, L6) exhibited comparable stability under acidic conditions, with L4 clearly favored above pH 3.5 up to pH 6, which is in agreement with the number of deprotonated Asp and His residues and has been discussed in previous competitions. For L2*, once again, we observed a typical increase in the stability of formed complexes together with the number of deprotonated His residues and the possibility to form polymorphic species.[20] Above pH = 7, when water molecules in the coordination sphere of Mn(II) ions start to deprotonate, the L6 ligand clearly forms the most stable complexes with Mn(II) ions. As L6 is the only fully polycarboxylate ligand investigated in this study, currently it is difficult to explain this behavior, and further studies are needed.

This competition plot (Fig. 5) once again highlights the pH-dependent coordination preferences of Mn(II) ions, with pronounced preferences for clustered binding motifs. In the acidic pH, the complex stability is influenced not only by the number of available Asp residues, but also their position and overall electrostatic environment. This example showcases how highly nuanced and multifactorial the coordination preferences of Mn(II) can be.

For Fe(II) complexes, L5* is the most stable ligand across the entire pH range, consistent with Fe(II)'s strong preference for adjacent Asp and His residues (Fig. 5). The L6 ligand maintains comparable stability to L5* up to pH 6, after which its stability declines. Above pH 6 the number of deprotonated His residues in the case of L5* increases, while for L6 only deprotonation of H_2O molecules occur. The involvement of His residues improves the stability of Fe(II) complexes in the case of L5*. Between pH 7–8.5, the L2* and L4 ligands showcase negligible stability in comparison to L5*. This competition once again underlines the preferences of Fe(II) ions to mixed O/N donor atoms in the coordination sphere. The alternating arrangement of these residues is of importance.

The increased number of oxygen donor atoms in poly-His peptide sequences does not significantly affect the affinity of the ligands toward Mn(II) ions. As demonstrated in our previous work, it is more crucial for Mn(II) to have access to multiple binding sites, as a higher number of deprotonated residues provides additional coordination possibilities. The overall architecture of the ligand has proven to be more important than the mere presence of suitable donor groups, with Mn(II) favoring ligands containing clustered Asp and His residues. In general, complex stability increased with the size of the clusters present in the ligand. These results suggest that Mn(II) ions prefer peptide ligands featuring motifs that allow for flexible, polymorphic binding, rather than rigid, well-organized architectures. This behavior aligns with the known high kinetic lability of Mn(II), as flexible coordination allows dynamic exchange among donor atoms within a single ligand, thereby stabilizing the complex.[60–62] For Fe(II) ions, the thermodynamic stability of the complexes does not increase with the number of oxygen donor atoms; the presence of His residues is equally important, particularly for maintaining complexes' stability in higher pH. These findings indicate a strong preference of Fe(II) ions for mixed N/O coordination environments, with a notable tendency to form highly stable complexes involving adjacent Asp–His motifs. Competition plots further demonstrated that ligands with clustered Asp or His residues became progressively less effective as the cluster size increased. In the case of both metal ions, the high stability of L6 ligand complexes demonstrate that the absence of His and deviation from the ideal arrangement does not necessarily compromise complex stability. These observations underscore the nuanced and multifactorial nature of metal–peptide interactions and the need to evaluate each system within its unique context. Ligands rich in His residues and featuring clustered amino acid motifs formed the most stable complexes with Zn(II) ions. This behavior is typical for Zn(II) coordination chemistry and aligns well with established literature;[11,28,54,55] therefore, it was not discussed in detail here.

Conclusions

This study offers new insight into the underexplored coordination preferences of Mn(II) and Fe(II) ions in their interactions with model peptides. Our results emphasize the critical role of ligand sequence architecture and donor atom distribution in dictating metal selectivity and complex stability.

The main findings of this work regarding the overall binding preferences of Mn(II) and Fe(II) ions were; (a) for Mn(II)

ions the clustered architecture of the ligand is more important than the presence of suitable donor groups, as it allows for greater flexibility and a wider range of coordination possibilities with the metal ion, while for Fe(II) ions the affinity for more separated, neighboring His/Asp motifs was observed. The smaller the cluster, the higher the stability of a formed complex; (b) Mn(II)'s coordination preferences were strongly pH-dependent – in acidic, and basic pH there was a pronounced preference for acid-containing ligands, while in the vicinity of a neutral pH the number of available binding sites became more important, while Fe(II) displayed similar preferences through the entire pH-range; (c) for both metal ions the overall charge of the complex was important, favoring the greater negative charge of the ligand and the number of available binding sites.

These findings contribute to the fundamental understanding necessary for the rational design of peptide-based metal chelators, particularly in contexts requiring precise control over coordination environments. The spectroscopic silence of Mn(II)/Fe(II), combined with the complexity of His/Asp-rich peptides and difficulties in obtaining crystals limit precise identification of donor atoms and binding models. Therefore, studies of additional peptides, derived as direct fragments from Mn(II), Fe(II) and Zn(II)-binding proteins, are currently underway in our laboratory to further validate and expand these observations. Future investigations may also explore longer peptide sequences, modulate cluster size, or incorporate non-natural amino acids to further refine metal selectivity and binding affinity under biologically relevant conditions.

Author contributions

Karolina Pawlik: conceptualization, investigation, visualization, formal analysis, writing – original draft, writing – review & editing. Malgorzata Ostrowska: conceptualization, investigation, visualization, formal analysis, writing – original draft, writing – review & editing, funding acquisition, project administration, supervision. Elzbieta Gumienna-Kontecka: writing – review & editing, supervision.

Conflicts of interest

The authors declare no competing financial interest.

Data availability

The authors state that the data used to prepare the manuscript is stored in RODBUK Cracow Open Research Data Repository of University of Wroclaw and can be accessed through DOI: https://doi.org/10.34616/O9ZGT2.

Supplementary Information (SI), containing hydrolysis constants for the studied metal ions, ligand speciation diagrams, MS spectra of selected peptide complexes, EPR spectra of all Mn(II) systems in various pH, a description of the deprotonation pattern and coordination preferences of Zn(II) complexes together with their speciation diagrams and tables, as well as competition plots and analysis of their coordination properties, is available. See DOI: https://doi.org/10.1039/d6dt00180g.

Acknowledgements

We acknowledge the Polish National Science Centre (NCN, UMO-2021/43/D/ST4/01231) for the financial support.

References

1 J. Tainer, V. Roberts and E. Getzoff, Metal-Binding Sites in Proteins, *Curr. Opin. Biotechnol.*, 1991, **2**, 582–591.
2 K. Handing, E. Niedzialkowska, I. Shabalin, M. Kuhn, H. Zheng and W. Minor, *Nat. Protoc.*, 2018, **13**, 1062–1090.
3 R. De Ricco, S. Potocki, H. Kozlowski and D. Valensin, *Coord. Chem. Rev.*, 2014, **269**, 1–12.
4 M. Matzapetakis, D. Ghosh, T. Weng, J. Penner-Hahn and V. Pecoraro, *J. Biol. Inorg. Chem.*, 2006, **11**, 876–890.
5 T. Takahashi, B. Ngo, L. Xiao, G. Arya and M. Heller, *J. Biomol. Struct. Dyn.*, 2016, **34**, 463–474.
6 D. Arus, N. Nagy, A. Dancs, A. Jancsó, R. Berkecz and T. Gajda, *J. Biol. Inorg. Chem.*, 2013, **126**, 61–69.
7 H. Kozlowski, T. Kowalik-Jankowska and M. Jezowska-Bojczuk, *Coord. Chem. Rev.*, 2005, **249**, 2323–2334.
8 P. Faller and C. Hureau, *Dalton Trans.*, 2009, **7**, 1080–1094.
9 A. Rola, E. Gumienna-Kontecka and S. Potocki, *Dalton Trans.*, 2024, **53**(9), 4054–4066.
10 A. Grenács and I. Sóvágó, *J. Inorg. Biochem.*, 2014, **139**, 49–56.
11 K. Garstka, D. Bellotti, J. Watly, H. Kozlowski, M. Remelli and M. Rowinska-Zyrek, *Dalton Trans.*, 2023, **52**, 16140–16150.
12 V. Dzyhovskyi, M. Remelli and K. Stokowa-Soltys, *J. Inorg. Biochem.*, 2025, **263**, 112769.
13 C. Murdoch and E. Skaar, *Nat. Rev. Microbiol.*, 2022, **20**, 657–670.
14 M. Remelli, M. Peana, S. Medici, M. Ostrowska, E. Gumienna-Kontecka and M. A. Zoroddu, *Dalton Trans.*, 2016, **45**, 5151–5161.
15 M. Peana, S. Medici, H. A. Pangburn, T. J. Lamkin, M. Ostrowska, E. Gumienna-Kontecka and M. A. Zoroddu, *J. Inorg. Biochem.*, 2016, **164**, 49–58.
16 M. Peana, E. Gumienna-Kontecka, F. Piras, M. Ostrowska, K. Piasta, K. Krzywoszynska, S. Medici and M. A. Zoroddu, *Inorg. Chem.*, 2020, **59**, 4661–4684.
17 B. Orzel, A. Pelucelli, M. Ostrowska, S. Potocki, H. Kozlowski, M. Peana and E. Gumienna-Kontecka, *Inorg. Chem.*, 2023, **62**, 18607–18624.
18 B. Orzel, M. Ostrowska, S. Potocki, M. Zoroddu, H. Kozlowski, M. Peana and E. Gumienna-Kontecka, *Inorg. Chem.*, 2025, **64**, 5038–5052.

19 B. Orzel, M. Ostrowska, S. Potocki, H. Kozlowski, M. Peana and E. Gumienna-Kontecka, *Dalton Trans.*, 2025, **54**, 14779–14789.
20 K. Pawlik, M. Ostrowska and E. Gumienna-Kontecka, *Inorg. Chem.*, 2025, **64**, 5472–5486.
21 V. Jószal, Z. Nagy, K. Osz, D. Sanna, G. Di Natale, D. La Mendola, G. Pappalardo, E. Rizzarelli and I. Sóvagó, *J. Inorg. Biochem.*, 2006, **100**, 1399–1409.
22 J. Lv, R. Ingle, H. Wu, C. Liu and W. Fang, *Int. J. Pharm.*, 2024, **662**, 124472.
23 D. Witkowska, M. Rowinska-Zyrek, G. Valensin and H. Kozlowski, *Coord. Chem. Rev.*, 2012, **256**, 133–148.
24 G. R. Grimsley, J. M. Scholtz and C. N. Pace, *Protein Sci.*, 2009, **18**, 247–251.
25 R. Thurlkill, G. Grimsley, J. Scholtz and C. Pace, *Protein Sci.*, 2006, **15**, 1214–1218.
26 M. Rowinska-Zyrek, D. Witkowska, S. Potocki, M. Remelli and H. Kozlowski, *New J. Chem.*, 2013, **37**, 58–70.
27 K. Garstka, G. Potoczniak, H. Kozlowski and M. Rowinska-Zyrek, *Dalton Trans.*, 2024, **53**, 2848–2858.
28 D. Bellotti, S. Leveraro, A. Hecel and M. Remelli, *Anal. Biochem.*, 2023, **680**, 115315.
29 I. Poon, K. Patel, D. Davis, C. Parish and M. Hulett, *Blood*, 2011, **117**, 2093–2101.
30 F. Pontecchiani, E. Simonovsky, R. Wieczorek, N. Barbosa, M. Rowinska-Zyrek, S. Potocki, M. Remelli, Y. Miller and H. Kozlowski, *Dalton Trans.*, 2014, **43**, 16680–16689.
31 P. Favreau, O. Cheneval, L. Menin, S. Michalet, H. Gaertner, F. Principaud, R. Thai, A. Ménez, P. Bulet and R. Stöcklin, *Rapid Commun. Mass Spectrom.*, 2007, **21**, 406–412.
32 A. Hecel, K. Garstka, H. Kozlowski and M. Rowinska-Zyrek, *J. Inorg. Biochem.*, 2024, **252**, 112456.
33 A. Miller, A. Matera-Witkiewicz, A. Mikolajczyk, J. Watly, D. Wilcox, D. Witkowska and M. Rowinska-Zyrek, *Int. J. Mol. Sci.*, 2021, **22**, 6903.
34 T. Aiyelabola, E. Akinkunmi, I. Ojo, E. Obuotor, C. Adebajo and D. Isabirye, *Bioinorg. Chem. Appl.*, 2017, **2017**, 956145.
35 G. D'Abrosca, L. Russo, M. Palmieri, I. Baglivo, F. Netti, I. de Paola, L. Zaccaro, B. Farina, R. Iacovino, P. Pedone, *et al.*, *J. Inorg. Biochem.*, 2016, **161**, 91–98.
36 W. Butler, *Eur. J. Oral Sci.*, 1998, **106**, 204–210.
37 K. Gu, S. Chang, M. Slaven, B. Clarkson, R. Rutherford and H. Ritchie, *Eur. J. Oral Sci.*, 1998, **106**, 1043–1047.
38 R. van der Lee, M. Buljan, B. Lang, R. Weatheritt, G. Daughdrill, A. Dunker, M. Fuxreiter, J. Gough, J. Gsponer, D. Jones, *et al.*, *Chem. Rev.*, 2014, **114**, 6589–6631.
39 J. Gsponer and M. Babu, *Cell Rep.*, 2012, **2**, 1425–1437.
40 G. Gran, *Acta Chem. Scand.*, 1950, **4**, 559–577.
41 P. Gans and B. O'Sullivan, *Talanta*, 2000, **51**, 33–37.
42 P. Gans, A. Sabatini and A. Vacca, *Talanta*, 1996, **43**, 1739–1753.
43 L. Alderighi, P. Gans, A. Ienco, D. Peters, A. Sabatini and A. Vacca, *Coord. Chem. Rev.*, 1999, **184**, 311–318.
44 P. L. Brown and C. Ekberg, *Hydrolysis of Metal Ions*, Wiley, 2016.
45 C. F. Baes and R. E. Mesmer, *Am. J. Sci.*, 1981, **281**, 935–962.
46 J. Galey, B. Decocklereverend, A. Lebkiri, L. Pettit, S. Pyburn and H. Kozlowski, *J. Chem. Soc., Dalton Trans.*, 1991, **9**, 2281–2287.
47 A. Rola, A. Kola, D. Valensin, O. Palacios, M. Capdevila, E. Gumienna-Kontecka and S. Potocki, *Dalton Trans.*, 2024, **53**, 6676–6689.
48 A. Rola, O. Palacios, M. Capdevila, D. Valensin, E. Gumienna-Kontecka and S. Potocki, *Inorg. Chem.*, 2023, **62**, 6893–6908.
49 H. Kozlowski, W. Bal, M. Dyba and T. Kowalik-Jankowska, *Coord. Chem. Rev.*, 1999, **184**, 319–346.
50 K. L. Shaw, G. R. Grimsley, G. I. Yakovlev, A. A. Makarov and C. N. Pace, *Protein Sci.*, 2001, **10**, 1206–1215.
51 J. Watly, E. Simonovsky, R. Wieczorek, N. Barbosa, Y. Miller and H. Kozlowski, *Inorg. Chem.*, 2014, **53**, 6675–6683.
52 J. Watly, E. Simonovsky, N. Barbosa, M. Spodzieja, R. Wieczorek, S. Rodziewicz-Motowidlo, Y. Miller and H. Kozlowski, *Inorg. Chem.*, 2015, **54**, 7692–7702.
53 S. Knecht, D. Ricklin, A. N. Eberle and B. Ernst, *J. Mol. Recognit.*, 2009, **22**, 270–279.
54 J. Watly, A. Hecel, M. Rowinska-Zyrek and H. Kozlowski, *Inorg. Chim. Acta*, 2018, **472**, 119–126.
55 J. Watly, K. Szarszon, A. Mikolajczyk, M. Grelich-Mucha, A. Matera-Witkiewicz, J. Olesiak-Banska and M. Rowinska-Zyrek, *Int. J. Mol. Sci.*, 2022, **23**, 15306.
56 S. Ray and R. Gaudet, *Biochem. Soc. Trans.*, 2023, **51**, 897–923.
57 F. A. Cotton, G. Wilkinson, C. A. Murillo and M. Bochmann, *Advanced Inorganic Chemistry*, Wiley, 1996.
58 A. Earnshaw and N. N. Greenwood, *Chemistry of the Elements*, Butterworth-Heinemann, 2nd edn, 1997.
59 R. Shannon, *Acta Crystallogr., Sect. A*, 1976, **32**, 751–767.
60 D. F. Shriver, P. W. Atkins and C. H. Langford, *Inorganic Chemistry*, W. H. Freeman, 1990.
61 Z. Garda, E. Molnár, F. Kálmán, R. Botár, V. Nagy, Z. Baranyai, E. Brücher, Z. Kovács, I. Tóth and G. Tircsó, *Front. Chem.*, 2018, **6**, 232.
62 G. Schanne, M. Zoumpoulaki, G. Gazzah, A. Vincent, H. Preud'homme, R. Lobinski, S. Demignot, P. Seksik, N. Delsuc and C. Policar, *Oxid. Med. Cell. Longevity*, 2022, **2022**, 8581222.